The Effect of Ligands and Transducers on the Neurotensin Receptor 1 (NTS1) Conformational Ensemble

Austin D. Dixon[§], Asuka Inoue[⊥], Scott A. Robson[§], Kelly J. Culhane[†], Jonathan C. Trinidad[‡], Sivaraj Sivaramakrishnan[†], Fabian Bumbak[§], and Joshua J. Ziarek[§*]

§Department of Molecular and Cellular Biochemistry, Indiana University, Bloomington, Indiana, USA 47405

⊥Graduate School of Pharmaceutical Sciences, Tohoku University, Sendai, Miyagi, Japan 980-8578

†Department of Genetics, Cell Biology, and Development, University of Minnesota, Minneapolis, Minnesota, USA 55455

‡Laboratory for Biological Mass Spectrometry, Indiana University, Bloomington, Indiana, USA 47405

Keywords: G protein-coupled receptors (GPCRs), allostery, nuclear magnetic resonance (NMR), membrane protein, saturation transfer difference (STD), ^{19}F

ABSTRACT: Using a discrete, intracellular ^{19}F-NMR probe on Neurotensin receptor 1 (NTS1) transmembrane helix (TM) 6, we aim to understand how ligands and transducers modulate the receptor's structural ensemble in solution. For apo NTS1, ^{19}F-NMR spectra reveal an ensemble of at least three states (one inactive and two active-like) in equilibrium that exchange on the ms-s timescale. Dynamic NMR experiments reveal that these substates follow a linear three-site exchange process that is both thermodynamically and kinetically remodeled by orthosteric ligands. As previously observed in other GPCRs, the full agonist is insufficient to completely stabilize the active state. Receptor coupling to β-arrestin-1 or the C-terminal helix of $G\alpha_q$, which comprises ≷60% of the GPCR/G protein interface surface area, abolishes the inactive substate. But whereas β-arrestin-1 selects for preexisting active-like substates, the $G\alpha_q$ peptide induces two new substates. Both transducer molecules promote substantial line-broadening of active states suggesting contributions from additional μs-ms exchange processes. Together, our study suggests i) the NTS1 allosteric activation mechanism is alternatively dominated by induced fit or conformational selection depending on the coupled transducer, and ii) the available static structures do not represent the entire conformational ensemble observed in solution.

INTRODUCTION

G protein-coupled receptors (GPCRs) serve as the primary hubs to relay changes in extracellular environments across the eukaryotic cell membrane.[1] The more than 800 members of this protein superfamily share a conserved seven transmembrane helix (TM) bundle architecture that recognizes a large variety of ligands comprising small molecules, hormones, peptides, and photons.[2] As such, it's no surprise they encompass over 30% of the drug market.[3] Although atomic models are still relatively scarce compared to other protein classes, there are currently 111 unique receptors structures, or ~13% of the total GPCR superfamily.[4] The Neurotensin receptor 1 (NTS1) has quickly become one of the most well-characterized Class A GPCRs with structures of the apo state, complexes with various pharmacological ligands, and ternary complexes with both the heterotrimeric Gq protein and β-arrestin-1 (βArr1) transducers.[5–9]

The difficulty of GPCR structural studies is primarily due to inherent poor protein stability and expression. Through the use of detergent membrane mimetics and creative receptor engineering, the rate at which new receptor structures are determined has increased in recent years.[10] These novel atomic models have revealed conserved, long-range allosteric activation networks that link the receptor orthosteric pocket to the intracellular bundle across the cell membrane. Most notably the DRY, PIF, and NPxxY motifs serve as internal molecular "switches", connecting ligand-binding to down-stream effector molecule complexation and activation events, spanning a distance of nearly 50 Å.[11] Modeling of allosteric switches across receptors has provided a canonical structural activation profile.[12,13]

A hallmark of GPCR activation is the outward movement of transmembrane helix 6 (TM6) to accommodate G protein and arrestin complexation.[5] In NTS1, the intracellular tip of TM6 undergoes a >13 Å lateral displacement upon ligand binding and subsequent transducer coupling.[6] Displacement of TM6 is allosterically linked to the orthosteric binding pocket; it has been shown that upon agonist binding, the volume of the extracellular vestibule of NTS1 decreases by 50%, coinciding with an increase in intracellular cavity volume mediated in part by TM6 translation.[5] A peptide-binding GPCR, NTS1 is found throughout the central nervous system and gastrointestinal tract with roles in regulating body temperature, mood, and GI motility.[14] NTS1 activation is mediated through binding of the neuropeptide neurotensin, which can potentiate hypothermia and analgesia, and is important to ongoing biochemical research for its pathogenesis in Parkinson's, Schizophrenia, obesity, hypotension, and methamphetamine addiction, amongst others.[15]

Current atomic models derived from either X-ray crystallography or cryo-EM capture NTS1 in different stages of activation, mediated by bound ligands and transducer proteins. Ultimately, those models remain static. This has left a void in the literature detailing the kinetic exchange of NTS1 substates and

the pleiotropic effects ligands and transducers have on the conformational ensemble of the TM bundle. This inspired us to pursue an orthogonal structural approach to better characterize the allosteric activation mechanism in NTS1. We took advantage of NMR spectroscopy, which offers the unique opportunity to observe inherent protein plasticity, exchange between conformers, and the allosteric influence drugs and other molecules have in effecting the structure-function relationship in solution.[16] In this study, we utilize ^{19}F-NMR spectroscopy on an evolved construct to develop a dynamic model of NTS1 activation, in which ligands and transducers are allosterically coupled.

RESULTS

Thermostabilized neurotensin receptor 1 retains signaling activity. The well-characterized structure of NTS1 in a variety of pharmacologically-relevant states creates an ideal system for exploring the allosteric mechanisms of GPCR activation. Yet, wildtype NTS1 structural characterization remains challenging due to poor receptor stability following isolation from native membranes.[17] All published NTS1 structures to date incorporate some combination of thermostabilizing mutations, lysozyme fusions, DARPin fusions, or conformationally-selective antibodies.[5,7,8,18] Here, we employed a functional, thermostabilized rat NTS1 variant (termed enNTS1) for solution NMR spectroscopy.[19]

To further characterize enNTS1's functional integrity, we performed a cell-based alkaline phosphatase (AP) reporter assay for G protein activation. Stimulation of $G\alpha_q$ and $G\alpha_{12/13}$ leads to ectodomain shedding of an AP-fused transforming growth factor-α (TGFα), which is then quantified using a colorimetric reporter.[20] HEK293 cells were transfected with AP-TGFα and a NTS1 plasmid construct. A hexapeptide corresponding to residues 8-13 of the neurotensin agonist (NT8-13) is sufficient to generate a full agonist response in wildtype rNTS1;[21] NT8-13 stimulates robust, concentration-dependent G protein-coupling to enNTS1 in the TGFα shedding assay, though with reduced efficacy compared to human (h)NTS1 (Figure 1A and Figure S1). Both enNTS1 and hNTS1 were equally expressed on the cell surface (Figure S1C). βArr1 recruitment was also measured via NanoBiT enzyme complementation system.[22] The large and small fragments of the split luciferase were fused to the N-terminus of βArr1 and the C-terminus of NTS1, respectively, and these constructs were expressed in HEK293 cells. As a negative control, we used the vasopressin V2 receptor (V2R) C-terminally fused with the small luciferase fragment. enNTS1 exhibited strong basal βArr1 recruitment that did not increase upon agonist addition (Figure 1B and Figure S1).

^{19}F-NMR probe does not affect enNTS1 function. To characterize enNTS1's structural ensemble in solution, we developed protocols to selectively-incorporate cysteine-reactive ^{19}F-NMR probes onto TM6. Many previous ^{19}F-NMR studies of GPCRs target position 6.27 (Ballesteros-Weinstein nomenclature), but coupling the ^{19}F-2-Bromo-N-(4-(trifluoromethyl)phenyl)acetamide (BTFMA) probe at this site reduced enNTS1 expression yields and stability (data not shown).[23–25] MtsslWizard was used to model cysteine-conjugated BTFMA probes at various alternative positions along TM6 of the apo (PDB 6Z66), agonist NT8-13-bound (PDB 4BWB), antagonist SR142948-bound (PDB 6Z4Q), $G\alpha_i\beta\gamma$ protein ternary (PDB 6OS9), and βArr1 ternary NTS1 complex structures (PDB 6UP7 and 6PWC).[5–9,26] MtsslWizard rapidly screened 200 randomly-generated BTFMA rotamers and enumerated all conformers that did not clash with the receptor to a tolerance of 3.4 Å. While position 6.27 is unrestricted in antagonist and transducer-bound models, the tight TM5/TM6 packing of the apo and agonist-bound structures sterically-restricted BTFMA to 18 and 110 potential rotamers, respectively, suggesting a mechanism for its observed instability (Figure S2A). In contrast, the neighboring residue Q301C$^{6.28}$ presented completely unhindered mobility in all six structural models (Figure S2A and Table S1). BTFMA-labeling at position 6.28 had no effect on receptor thermostability or yield.

In the final construct, herein enNTS1[Q301C^{BTFMA}], solvent exposed C172$^{3.55}$ was mutated to serine to prevent off-site labeling. Site-specific BTFMA labeling was confirmed by LC/MS and NMR with estimated efficiencies of >95% and >80%, respectively, with no observable off-site labeling (Figure S2B,C and Table S2). enNTS1[Q301C^{BTFMA}] showed no appreciable difference in affinity for agonist NT8-13 in saturation binding experiments compared to unlabeled enNTS1, indicative of proper receptor fold (Figure S2D). Dynamic NMR experiments require the sample to be stable during multiday data acquisition. To confirm enNTS1[Q301C^{BTFMA}] would remain viable during extended periods of data collection, we measured its ability to bind fluorescent agonist NT8-13 as a function of time. After ten days at 37 °C, 55.0 ± 5.7% apo and 82.1 ± 17.1% agonist-bound enNTS1[Q301C^{BTFMA}] preserved binding competency (Figure S3).

enNTS1's conformational ensemble is sensitive to orthosteric ligands. We collected 1D ^{19}F-NMR spectra of enNTS1[Q301C^{BTFMA}] in the absence and presence of saturating (10:1 Meq) orthosteric ligand concentrations to investigate the conformational ensemble. Spectral deconvolution of ligand-free enNTS1[Q301C^{BTFMA}] best-fit three Lorentzian lines indicating a three-state equilibrium in slow (ms-s) exchange on the NMR timescale, with S/N ratios ranging from 95.5 to 199.1 (Figure 1C). The area, chemical shift, and linewidth at half-height (LWHH) for each deconvoluted resonance serve as direct reporters of the relative population, chemical environment, and flexibility of each conformer, respectively.[27] Following the approach established by Prosser and colleagues, best-fit values were identified by individually constraining a given state's chemical shift over a range of frequencies and then globally-fitting the remaining parameters (Figure 1D).[24]

In the apo state, the three resonances (labeled S_1, S_2, and S_3) were populated at 5%, 80%, and 15%, respectively. The S_1 and S_3 LWHHs averaged ~300 Hz, nearly double the corresponding S_2 linewidth, which suggests contributions from μs-ms exchange processes (Figure 1C). The same three states were also present in agonist- and antagonist-bound spectra; agonist reduced the S_1 population while increasing S_2, whereas antagonist had the opposite effect (Figure 1C). Both ligands similarly decreased the S_1 LWHH ~20 Hz suggesting a slight stabilizing effect. The S_2 state exhibited subtle ligand-dependent frequency perturbations – shifting approximately 0.01 ppm downfield and 0.04 ppm upfield in response to SR142948 antagonist and NT8-13 agonist, respectively (Figure 1C). The simplest explanation for this behavior is an exchanging two-state equilibrium where the peak position reflects the relative population of each state; the exchange process is likely on the millisecond timescale assuming the frequency difference between the two pure substates is $\lessapprox$ 200 Hz. These modest chemical shift perturbations were accompanied by ~20 Hz line broadening. Similarly, the S_3

linewidth reported on ligand-efficacy with agonist decreasing, and antagonist increasing, the LWHH by 20 Hz (Figure 1C).

We hypothesize that S_1 is an inactive state whereas S_2 and S_3 reflect active-like states. This is based upon several similar observations with other receptors: i) the comparatively broad S_1 linewidth, which is consistent with μs-ms timescale motions such as ionic lock flickering between formation/disruption reported for the β_2-, β_1-adrenergic, and A_{2A} adenosine receptors;[28–30] ii) the near disappearance of the S_1 resonance and concurrent increase of the S_2 population upon agonist addition; iii) the S_1, S_2, and S_3 substate chemical shifts are increasingly upfield, which is consistent with increased solvent exposure as the cytoplasmic cavity expands for transducer association.[25,31]

Orthosteric ligands modulate distinct conformational kinetics. The simultaneous observation of three distinct enNTS1[Q301C^{BTFMA}] resonances defines an upper limit of approximately 10^{-3} s^{-1} to the exchange rates. We undertook saturation transfer difference (STD) dynamic NMR experiments to quantify the exchange kinetics between substates. STD experiments employ a low power pulse to selectively saturate (i.e. reduce the intensity) a single substate frequency, ν_s. When a saturated substate exchanges, it decreases the signal at the other site(s). A series of 1D spectra were collected with the saturation pulse duration varied from 50-1000 ms. To account for off-resonance saturation effects, a second series of 1D spectra were collected with a control saturation pulse set at an equal, but opposite, offset (ν_c) from the substate of interest. The difference in peak height between on- and off-resonance experiments ($\nu_{s,eff}$), as a function of saturation pulse length, can be fitted to yield the exchange rate constant (k) with the irradiated resonance, and by extension the lifetimes ($\tau_s = 1/k$) of each conformer (Figure S4, Table S3).

The three enNTS1[Q301C^{BTFMA}] substates exhibited lifetimes ranging from 10-4000 ms depending on the ligand-state of the receptor. STD experiments revealed that the S_2 substate is long-lived for apo receptor (2.40 s) in exchange with S_1, whereas it exchanges over three times as fast with S_3 (0.67 s) (Figure 2). This agrees with the population percentages extracted from our 1D experiments where S_2 is the dominant conformer. Interestingly, in the presence of NT8-13 the lifetimes of both S_2 and S_3 are shortened (0.01-0.04 s) and S_1 increased (1.67 s), suggesting the agonist energetically biases the receptor towards substate S_1 (Figure 2). Antagonist SR142948 exerts most of its effects on the exchange of S_2 to S_3 with a marked life-time increase (3.99 s) which may be the result of an allosteric increase in the energy barrier between the substates (Figure 2). In all three liganded states we were unable to observe direct exchange between S_1 and S_3 (Figure S5), which supports a linear activation trajectory ($S_1 \rightarrow S_2 \rightarrow S_3$) from the inactive conformer to the most solvent exposed position (Figure S4 and Table S3). Such a sequential transition has also been observed for ^{19}F-TM6$^{6.27}$ of the adenosine A_{2A} receptor.[30]

G protein mimetic stabilizes novel conformations. Next, we investigated the interaction of enNTS1 with a synthetic peptide (herein $G\alpha_q$ peptide) corresponding to residues 333-359 of the $G\alpha_q$ C-terminus (a.k.a. α5-helix). The α5-helix is conserved across G proteins as a random coil that adopts a helical structure upon receptor recognition to comprise 55-69% of the GPCR/G protein interface surface area.[32–34] We first characterized the efficacy of the enNTS1/$G\alpha_q$ peptide interaction using an affinity pulldown approach.[35] The $G\alpha_q$ peptide was N-terminally fused to a biotin tag and enNTS1 contained a C-terminal monomeric, ultra-stabilized green fluorescent protein (muGFP) fusion (enNTS1-muGFP).[36] Binding efficacy was quantified as the fluorescence ratio of streptavidin-captured enNTS1-muGFP versus total (i.e. streptavidin-captured plus unbound) fluorescence. In the absence of a ligand, the $G\alpha_q$ peptide captured 26.2 ± 6.4% apo enNTS1-muGFP, which is consistent with β_2-adrenergic receptor basal activity observed previously using the same experimental approach.[35] Repeating the pulldown in the presence of saturating NT8-13 agonist increased the enNTS1-muGFP capture efficiency to 36.4 ± 6.4% whereas the SR142948 antagonist had no significant effect (Figure 3A). Repeating the experiment with enNTS1[Q301C^{BTFMA}] showed no appreciable differences from enNTS1, indicating that the TM6 ^{19}F-BTFMA label does not influence $G\alpha_q$ peptide interaction (Figure 3A).

The $G\alpha_q$ peptide strikingly modified the NT8-13-bound enNTS1[Q301C^{BTFMA}] ^{19}F-NMR spectra by replacing the three substates S_1, S_2 and S_3 with two unique chemical shifts at 13.95 ($S_{2'}$) and 13.26 ppm (S_4) (Figure 3B and Figure S6). Labeling the downfield resonance as $S_{2'}$ reflects our hypothesis that the S_2 substate is an active-like state in fast-exchange on the NMR timescale. Formation of the $G\alpha_q$ peptide ternary complex increases the $S_{2'}$ population to 88.1% compared to 83.6% S_2 for NT8-13-bound, and the increase in linewidth from 166 Hz to 223 Hz reflects amplified μs-ms timescale exchange. The $G\alpha_q$ peptide-induced S_4 substate is upfield of any ligand-only conformer consistent with previous studies that agonist alone is unable to completely stabilize the fully active conformation.[37] The S_4 resonance linewidth is 372 Hz and constitutes 11.9% of the observed populations (Figure 3E).

A similar distribution of TM6 G protein-bound conformers has also been observed for the adenosine A_{2A} receptor in complex with $G\alpha_s$ peptide via ^{19}F-NMR.[38] Once bound to the stimulatory G protein peptide and cognate agonist, TM6 populated two distinct conformers at the expense of all inactive substates. A concurrent population increase for the upfield-most chemical shift occurred, similar to S_4 for enNTS1[Q301C^{BTFMA}]. It is possible that for a majority of class-A GPCRs complexation with G proteins induce μs-ms timescale chemical exchange of TM6 reflecting pre-coupling conformations prior to full receptor stimulation.

Arrestin stabilizes preexisting conformations. We next wanted to test if βArr1 modified the enNTS1 intracellular landscape similar to the $G\alpha_q$ peptide. βArr1 recruitment is physiologically-dependent on receptor phosphorylation, primarily on intracellular loop 3 (ICL3) and the C-terminus, but the number and location of sites necessary and sufficient to promote coupling is relatively unknown.[39] To reduce system complexity and facilitate a high-affinity interaction, we employed a pre-activated human βArr1 that was truncated at N382 (herein βArr1[ΔCT]).[40] Microscale thermophoresis (MST) was used to determine the apparent equilibrium dissociation constants (K_d) of enNTS1[Q301C^{BTFMA}]/βArr1[ΔCT] complexes. The N-terminal His-tag of βArr1[ΔCT] was site-specifically labeled with the RED-tris-NTA 2nd Generation (Monolith) fluorescent dye. RED-βArr1[ΔCT] was then incubated with increasing enNTS1[Q301C^{BTFMA}] concentrations in the presence or absence of saturating NT8-13 agonist. The interactions followed a sigmoidal dose-response and affinities were calculated using the quadratic binding model. Apo enNTS1[Q301C^{BTFMA}] bound RED-βArr1[ΔCT] with K_d = 506.2 ± 48 nM consistent with the high-affinity reported for pre-activated arrestin variants (Figure

3C).[6,41] The NT8-13 agonist increased affinity to 90.6 ± 5.8 nM, which is similar to the NTS1:Gαiβγ ternary complex in phospholipid nanodiscs.[42]

Analogous to the $G\alpha_q$ peptide, βArr1[ΔCT] abolished the inactive S_1 substate (Figure 3D). But rather than inducing a new substate resonance, βArr1[ΔCT] selectively restructured the existing conformational landscape by increasing the S_3 population to 27.7% and decreasing S_2 to 72.3% (Figure 3D). The linewidths of S_2 and S_3 increased to 237 Hz and 376 Hz, respectively, further reflecting the increased contributions of μs-ms timescale chemical exchange (Figure 3D).

DISCUSSION

The spectroscopic results shown here indicate the cytosolic cavity of enNTS1 dynamically populates an ensemble of at least three conformers that are allosterically-tuned across the cell membrane from the orthosteric pocket. As shown for other class-A GPCRs, agonist binding in enNTS1 does not stabilize a single active conformation but rather tunes the energetic landscape of inactive and active states. Even in the apo state, enNTS1 populates arrestin-competent conformers consistent with the basal activity in our cellular assays and is supportive of previous models (Figure 1B).[43] Inspection of all 24 antagonist-, agonist-, and transducer-bound NTS1 atomic models can be roughly organized into three substates (inactive, active-intermediate, and active) based upon the position of TM6 relative to TM4 (Figure S7). We speculate the observed NMR states represent these structural categories. Future studies may require distance measurements using DEER or florescence spectroscopy to further supplement our observed NMR states. As such, the atomic structures of NTS1 directly align with the ensemble observed in our ^{19}F-NMR spectra of enNTS1[Q301C^{BTFMA}] and suggest a model for activation (Figure 4).

Similar to orthosteric ligands, the enNTS1[Q301C^{BTFMA}] ensemble in complexation with agonist and transducer βArr1[ΔCT] conformationally selects between active states (Figure 3D). The abolition of inactive conformers likely arises from steric perturbance between TM6 and the inserted finger-loop region of βArr1. The abolition of inactive S_1 substate upon ternary complexation with βArr1[ΔCT] aligns with previously published atomic models of NTS1/βArr1; insertion of an unstructured finger-loop by βArr1 into the cytosolic cavity of NTS1 sterically precludes population of TM6 to the inactive conformer.[6] The increase in resonance linewidth for both populated substates is likely related to fast-exchange interactions between the inserted finger-loop and TM6, as well as between ICL3 and the positively charged N-terminal domain of βArr1; ICL3 connects transmembrane helices 5 and 6, and has been shown to form interactions with βArr1 necessary for ternary complexation.[9] In contrast, the C-terminal helix of $G\alpha_q$, which comprises ≳60% of the GPCR/transducer interface surface area, induces two active substates distinct from those observed for orthosteric ligands alone or with βArr1 (Figure 3B). While both transducers dock helical motifs into the cytosolic core of the receptor, the orientation of each segment is structurally unique; the inserted βArr1 finger-loop is 90° relative to TM6 whereas the G protein α5 helix is parallel.[6,8] The discrete coordination of docking interfaces may induce subtle structural fluctuations of TM6 that are not easily captured in static models. Together, this suggests the enNTS1 allosteric activation mechanism may alternate between induced fit ($G\alpha_q$ peptide) and conformational selection (βArr1) depending on the coupled transducer.

Ultimately, orthosteric NTS1 ligands modulate energy barriers between substate conformers that directly impact both the exchange kinetics and relative populations, providing a foundation for the design of biased-ligands to select discrete NTS1 activation modes. Researchers have begun identifying on-target pathway associations between desired and unwanted affects in drug use; biased allosteric modulators (BAMs) of GPCRs, including NTS1, have been developed for the treatment of patients suffering from drug addiction and its related symptoms.[44] As this study has shown for enNTS1, allosteric fine-tuning of conformers is a well-regulated phenomenon for downstream stimulation of varying transducer molecules, and could be utilized as a targeted therapeutic. With the design of novel BAM molecules, a molecular understanding of the resulting conformational bias is required. The ^{19}F-NMR method developed in this study serves as a great platform for the initial delineation of BAM-induced NTS1 substates, as novel biased ligands have been developed for the treatment of methamphetamine abuse such as ML314 and SBI-553.[45]

A limitation of the ^{19}F-NMR method presented here is the inherent drawback of a single-site reporter, which is unable to connect global conformational and dynamic fluctuations. However, varying permutations of probe incorporation sites could be generated to supplement chemical shift information around the helical bundle. It is also important to note the lack of full-length G protein and arrestin constructs used in this study. Instead, we employed the C-terminal helix of $G\alpha_q$ and a pre-activated form of βArr1 that does not require receptor phosphorylation; these transducer modifications were utilized to ensure high-affinity and reproducible interaction between enNTS1 and transducer. While more experiments are required to further the dynamic NTS1 model presented here, this study illustrates the importance of orthogonal structural techniques in determining the mechanism of GPCR activation.

ASSOCIATED CONTENT

Detailed experimental procedures (PDF)

AUTHOR INFORMATION

Corresponding Author

*jjziarek@indiana.edu

ORCID

Austin D. Dixon: 0000-0001-8676-915X
Asuka Inoue: 0000-0003-0805-4049
Scott A. Robson: 0000-0002-0529-0399
Kelly J. Culhane: 0000-0001-8075-4782
John C. Trinidad: 0000-0002-8279-1509
Sivaraj Sivaramakrishnan: 0000-0002-9541-6994
Joshua J. Ziarek: 0000-0002-3740-9999

Funding Sources

The project was funded by: Indiana Precision Health Initiative (JJZ), NIH grant R00GM115814 (JJZ), KAKENHI 21H04791 (A.I.), 21H051130 (A.I.), JPJSBP120213501 (A.I.) from Japan Society for the Promotion of Science (JSPS), LEAP JP20gm0010004 (A.I.), BINDS JP20am0101095 (A.I.) from the Japan Agency for Medical Research and Development (AMED), JST Moonshot Research and Development Program JPMJMS2023 (A.I.) from Japan Science and Technology Agency (JST), Daiichi Sankyo Foundation of Life Science (A.I.), Takeda Science Foundation (A.I.), Ono Medical Research Foundation (A.I.), Uehara Memorial Foundation (A.I.).

Notes

The authors declare no competing financial interests.

ACKNOWLEDGMENT

We are grateful to Prof. Gregor Hagelueken at the University of Bonn for assistance and modeling in the mtsslWizard software, Dr. Hongwei Wu at Indiana University for NMR instrument assistance, Dr. Ratan Rai at Indiana University School of Medicine for NMR instrument assistance, Kouki Kawakami at Tohoku University for technical assistance, and Kayo Sato, Shigeko Nakano and Ayumi Inoue at Tohoku University for their assistance in plasmid preparation and cell-based GPCR assays. The 14.1 T spectrometers used in this study was generously supported by the Indiana University Fund.

REFERENCE

(1) de Mendoza, A.; Sebé-Pedrós, A.; Ruiz-Trillo, I. The Evolution of the GPCR Signaling System in Eukaryotes: Modularity, Conservation, and the Transition to Metazoan Multicellularity. *Genome Biol. Evol.* **2014**, *6* (3), 606–619.

(2) Hanlon, C. D.; Andrew, D. J. Outside-in Signaling – a Brief Review of GPCR Signaling with a Focus on the Drosophila GPCR Family. *J. Cell Sci.* **2015**, *128* (19), 3533–3542.

(3) Hauser, A. S.; Attwood, M. M.; Rask-Andersen, M.; Schiöth, H. B.; Gloriam, D. E. Trends in GPCR Drug Discovery: New Agents, Targets and Indications. *Nat. Rev. Drug Discov.* **2017**, *16* (12), 829–842.

(4) Munk, C.; Isberg, V.; Mordalski, S.; Harpsøe, K.; Rataj, K.; Hauser, A. S.; Kolb, P.; Bojarski, A. J.; Vriend, G.; Gloriam, D. E. GPCRdb: The G Protein-Coupled Receptor Database - an Introduction. *Br. J. Pharmacol.* **2016**, *173* (14), 2195–2207.

(5) Mattia, D.; Alexander, K.; Christoph, K.; Lisa, M.; A., E. S.; Lena, M.; Philipp, H.; E., M. P. R.; Patrick, E.; M., K. T.; Yuanjun, H.; Santiago, V.; Pascal, E.; Annemarie, H.; Andreas, P. Complexes of the Neurotensin Receptor 1 with Small-Molecule Ligands Reveal Structural Determinants of Full, Partial, and Inverse Agonism. *Sci. Adv.* **2021**, *7* (5), eabe5504–eabe5504.

(6) Huang, W.; Masureel, M.; Qu, Q.; Janetzko, J.; Inoue, A.; Kato, H. E.; Robertson, M. J.; Nguyen, K. C.; Glenn, J. S.; Skiniotis, G.; Kobilka, B. K. Structure of the Neurotensin Receptor 1 in Complex with β-Arrestin 1. *Nature* **2020**, *579* (7798), 303–308.

(7) Egloff, P.; Hillenbrand, M.; Klenk, C.; Batyuk, A.; Heine, P.; Balada, S.; Schlinkmann, K. M.; Scott, D. J.; Schütz, M.; Plückthun, A. Structure of Signaling-Competent Neurotensin Receptor 1 Obtained by Directed Evolution in <Em>Escherichia Coli</Em> *Proc. Natl. Acad. Sci.* **2014**, *111* (6), E655 LP-E662.

(8) Kato, H. E.; Zhang, Y.; Hu, H.; Suomivuori, C.-M.; Kadji, F. M. N.; Aoki, J.; Krishna Kumar, K.; Fonseca, R.; Hilger, D.; Huang, W.; Latorraca, N. R.; Inoue, A.; Dror, R. O.; Kobilka, B. K.; Skiniotis, G. Conformational Transitions of a Neurotensin Receptor 1–Gi1 Complex. *Nature* **2019**, *572* (7767), 80–85.

(9) Yin, W.; Li, Z.; Jin, M.; Yin, Y.-L.; de Waal, P. W.; Pal, K.; Yin, Y.; Gao, X.; He, Y.; Gao, J.; Wang, X.; Zhang, Y.; Zhou, H.; Melcher, K.; Jiang, Y.; Cong, Y.; Edward Zhou, X.; Yu, X.; Eric Xu, H. A Complex Structure of Arrestin-2 Bound to a G Protein-Coupled Receptor. *Cell Res.* **2019**, *29* (12), 971–983.

(10) Grisshammer, R. New Approaches towards the Understanding of Integral Membrane Proteins: A Structural Perspective on G Protein-Coupled Receptors. *Protein Sci.* **2017**, *26* (8), 1493–1504.

(11) Schönegge, A.-M.; Gallion, J.; Picard, L.-P.; Wilkins, A. D.; Le Gouill, C.; Audet, M.; Stallaert, W.; Lohse, M. J.; Kimmel, M.; Lichtarge, O.; Bouvier, M. Evolutionary Action and Structural Basis of the Allosteric Switch Controlling B2AR Functional Selectivity. *Nat. Commun.* **2017**, *8* (1), 2169.

(12) Sanchez-Soto, M.; Verma, R. K.; Willette, B. K. A.; Gonye, E. C.; Moore, A. M.; Moritz, A. E.; Boateng, C. A.; Yano, H.; Free, R. B.; Shi, L.; Sibley, D. R. A Structural Basis for How Ligand Binding Site Changes Can Allosterically Regulate GPCR Signaling and Engender Functional Selectivity. *Sci. Signal.* **2020**, *13* (617).

(13) Zhou, Q.; Yang, D.; Wu, M.; Guo, Y.; Guo, W.; Zhong, L.; Cai, X.; Dai, A.; Jang, W.; Shakhnovich, E. I.; Liu, Z.-J.; Stevens, R. C.; Lambert, N. A.; Babu, M. M.; Wang, M.-W.; Zhao, S. Common Activation Mechanism of Class A GPCRs. *Elife* **2019**, *8*, e50279–e50279.

(14) Remaury, A.; Vita, N.; Gendreau, S.; Jung, M.; Arnone, M.; Poncelet, M.; Culouscou, J.-M.; Le Fur, G.; Soubrié, P.; Caput, D.; Shire, D.; Kopf, M.; Ferrara, P. Targeted Inactivation of the Neurotensin Type 1 Receptor Reveals Its Role in Body Temperature Control and Feeding Behavior but Not in Analgesia. *Brain Res.* **2002**, *953* (1), 63–72.

(15) Boules, M.; Li, Z.; Smith, K.; Fredrickson, P.; Richelson, E. Diverse Roles of Neurotensin Agonists in the Central Nervous System . *Frontiers in Endocrinology*. 2013, p 36.

(16) Tikhonova, I. G.; Costanzi, S. Unraveling the Structure and Function of G Protein-Coupled Receptors through NMR Spectroscopy. *Curr. Pharm. Des.* **2009**, *15* (35), 4003–4016.

(17) White, J. F.; Grisshammer, R. Stability of the Neurotensin Receptor NTS1 Free in Detergent Solution and Immobilized to Affinity Resin. *PLoS One* **2010**, *5* (9), e12579–e12579.

(18) White, J. F.; Noinaj, N.; Shibata, Y.; Love, J.; Kloss, B.; Xu, F.; Gvozdenovic-Jeremic, J.; Shah, P.; Shiloach, J.; Tate, C. G.; Grisshammer, R. Structure of the Agonist-Bound Neurotensin Receptor. *Nature* **2012**, *490* (7421), 508–513.

(19) Bumbak, F.; Keen, A. C.; Gunn, N. J.; Gooley, P. R.; Bathgate, R. A. D.; Scott, D. J. Optimization and 13CH3 Methionine Labeling of a Signaling Competent Neurotensin Receptor 1 Variant for NMR Studies. *Biochim. Biophys. Acta - Biomembr.* **2018**, *1860* (6), 1372–1383.

(20) Inoue, A.; Ishiguro, J.; Kitamura, H.; Arima, N.; Okutani, M.; Shuto, A.; Higashiyama, S.; Ohwada, T.; Arai, H.; Makide, K.; Aoki, J. TGFα Shedding Assay: An Accurate and Versatile Method for Detecting GPCR Activation. *Nat. Methods* **2012**, *9* (10), 1021–1029.

(21) García-Garayoa, E.; Bläuenstein, P.; Bruehlmeier, M.; Blanc, A.; Iterbeke, K.; Conrath, P.; Tourwé, D.; Schubiger, P. A. Preclinical Evaluation of a New, Stabilized Neurotensin(8--13) Pseudopeptide Radiolabeled with (99m)Tc. *J. Nucl. Med.* **2002**, *43* (3), 374–383.

(22) Dixon, A. S.; Schwinn, M. K.; Hall, M. P.; Zimmerman, K.; Otto, P.; Lubben, T. H.; Butler, B. L.; Binkowski, B. F.; Machleidt, T.; Kirkland, T. A.; Wood, M. G.; Eggers, C. T.; Encell, L. P.; Wood, K. V. NanoLuc Complementation Reporter Optimized for Accurate Measurement of Protein Interactions in Cells. *ACS Chem. Biol.* **2016**, *11* (2), 400–408.

(23) Ballesteros, J. A.; Weinstein, H. [19] Integrated Methods for the Construction of Three-Dimensional Models and Computational Probing of Structure-Function Relations in G Protein-Coupled Receptors. In *Receptor Molecular Biology*; Sealfon, S. C. B. T.-M. in N., Ed.; Academic Press, 1995; Vol. 25, pp 366–428.

(24) Kim, T. H.; Chung, K. Y.; Manglik, A.; Hansen, A. L.; Dror, R. O.; Mildorf, T. J.; Shaw, D. E.; Kobilka, B. K.; Prosser, R. S. The Role of Ligands on the Equilibria Between Functional States of a G Protein-Coupled Receptor. *J. Am. Chem. Soc.* **2013**, *135* (25), 9465–9474.

(25) Manglik, A.; Kim, T. H.; Masureel, M.; Altenbach, C.; Yang, Z.; Hilger, D.; Lerch, M. T.; Kobilka, T. S.; Thian, F. S.; Hubbell, W. L.; Prosser, R. S.; Kobilka, B. K. Structural Insights into the Dynamic Process of B2-Adrenergic Receptor Signaling. *Cell* **2015**, *161* (5), 1101–1111.

(26) Hagelueken, G.; Ward, R.; Naismith, J. H.; Schiemann, O. MtsslWizard: In Silico Spin-Labeling and Generation of Distance Distributions in PyMOL. *Appl. Magn. Reson.* **2012**, *42* (3), 377–391.

(27) CAVANAGH, J.; FAIRBROTHER, W. J.; PALMER, A. G.; RANCE, M.; SKELTON, N. J. CHAPTER 1 - CLASSICAL NMR SPECTROSCOPY; CAVANAGH, J., FAIRBROTHER, W. J., PALMER, A. G., RANCE, M., SKELTON, N. J. B. T.-P. N. M. R. S. Second E., Eds.; Academic Press: Burlington, 2007; pp 1–28.

(28) Liu, J. J.; Horst, R.; Katritch, V.; Stevens, R. C.; Wüthrich, K. Biased Signaling Pathways in B₂-

Adrenergic Receptor Characterized by ¹⁹F-NMR. *Science (80-.).* **2012**, *335* (6072), 1106 LP – 1110.

(29) Frei, J. N.; Broadhurst, R. W.; Bostock, M. J.; Solt, A.; Jones, A. J. Y.; Gabriel, F.; Tandale, A.; Shrestha, B.; Nietlispach, D. Conformational Plasticity of Ligand-Bound and Ternary GPCR Complexes Studied by 19F NMR of the B1-Adrenergic Receptor. *Nat. Commun.* **2020**, *11* (1), 669.

(30) Sušac, L.; Eddy, M. T.; Didenko, T.; Stevens, R. C.; Wüthrich, K. A_{2A} Adenosine Receptor Functional States Characterized by ¹⁹F-NMR. *Proc. Natl. Acad. Sci.* **2018**, *115* (50), 12733 LP – 12738.

(31) Hull, W. E.; Sykes, B. D. Fluorotyrosine Alkaline Phosphatase. Fluorine-19 Nuclear Magnetic Resonance Relaxation Times and Molecular Motion of the Individual Fluorotyrosines. *Biochemistry* **1974**, *13* (17), 3431–3437.

(32) Mobbs, J. I.; Belousoff, M. J.; Harikumar, K. G.; Piper, S. J.; Xu, X.; Furness, S. G. B.; Venugopal, H.; Christopoulos, A.; Danev, R.; Wootten, D.; Thal, D. M.; Miller, L. J.; Sexton, P. M. Structures of the Human Cholecystokinin 1 (CCK1) Receptor Bound to Gs and Gq Mimetic Proteins Provide Insight into Mechanisms of G Protein Selectivity. *PLOS Biol.* **2021**, *19* (6), e3001295–e3001295.

(33) Xia, R.; Wang, N.; Xu, Z.; Lu, Y.; Song, J.; Zhang, A.; Guo, C.; He, Y. Cryo-EM Structure of the Human Histamine H1 Receptor/Gq Complex. *Nat. Commun.* **2021**, *12* (1), 2086.

(34) Kim, K.; Che, T.; Panova, O.; DiBerto, J. F.; Lyu, J.; Krumm, B. E.; Wacker, D.; Robertson, M. J.; Seven, A. B.; Nichols, D. E.; Shoichet, B. K.; Skiniotis, G.; Roth, B. L. Structure of a Hallucinogen-Activated Gq-Coupled 5-HT(2A) Serotonin Receptor. *Cell* **2020**, *182* (6), 1574-1588.e19.

(35) Gupte, T. M.; Ritt, M.; Dysthe, M.; Malik, R. U.; Sivaramakrishnan, S. Minute-Scale Persistence of a GPCR Conformation State Triggered by Non-Cognate G Protein Interactions Primes Signaling. *Nat. Commun.* **2019**, *10* (1), 4836.

(36) Scott, D. J.; Gunn, N. J.; Yong, K. J.; Wimmer, V. C.; Veldhuis, N. A.; Challis, L. M.; Haidar, M.; Petrou, S.; Bathgate, R. A. D.; Griffin, M. D. W. A Novel Ultra-Stable, Monomeric Green Fluorescent Protein For Direct Volumetric Imaging of Whole Organs Using CLARITY. *Sci. Rep.* **2018**, *8* (1), 667.

(37) Weis, W. I.; Kobilka, B. K. The Molecular Basis of G Protein-Coupled Receptor Activation. *Annu. Rev. Biochem.* **2018**, *87*, 897–919.

(38) Ye, L.; Van Eps, N.; Zimmer, M.; Ernst, O. P.; Scott Prosser, R. Activation of the A2A Adenosine G-Protein-Coupled Receptor by Conformational Selection. *Nature* **2016**, *533*, 265.

(39) Sente, A.; Peer, R.; Srivastava, A.; Baidya, M.; Lesk, A. M.; Balaji, S.; Shukla, A. K.; Babu, M. M.; Flock, T. Molecular Mechanism of Modulating Arrestin Conformation by GPCR Phosphorylation. *Nat. Struct. Mol. Biol.* **2018**, *25* (6), 538–545.

(40) Vishnivetskiy, S. A.; Schubert, C.; Climaco, G. C.; Gurevich, Y. V; Velez, M. G.; Gurevich, V. V. An Additional Phosphate-Binding Element in Arrestin Molecule. Implications for the Mechanism of Arrestin Activation. *J. Biol. Chem.* **2000**, *275* (52), 41049–41057.

(41) Chen, Q.; Perry, N. A.; Vishnivetskiy, S. A.; Berndt, S.; Gilbert, N. C.; Zhuo, Y.; Singh, P. K.; Tholen, J.; Ohi, M. D.; Gurevich, E. V; Brautigam, C. A.; Klug, C. S.; Gurevich, V. V; Iverson, T. M. Structural Basis of Arrestin-3 Activation and Signaling. *Nat. Commun.* **2017**, *8* (1), 1427.

(42) Zhang, M.; Gui, M.; Wang, Z.-F.; Gorgulla, C.; Yu, J. J.; Wu, H.; Sun, Z. J.; Klenk, C.; Merklinger, L.; Morstein, L.; Hagn, F.; Plückthun, A.; Brown, A.; Nasr, M. L.; Wagner, G. Cryo-EM Structure of an Activated GPCR–G Protein Complex in Lipid Nanodiscs. *Nat. Struct. Mol. Biol.* **2021**, *28* (3), 258–267.

(43) Lamichhane, R.; Liu, J. J.; Pljevaljcic, G.; White, K. L.; van der Schans, E.; Katritch, V.; Stevens, R. C.; Wüthrich, K.; Millar, D. P. Single-Molecule View of Basal Activity and Activation Mechanisms of the G Protein-Coupled Receptor B₂AR. *Proc. Natl. Acad. Sci.* **2015**, *112* (46), 14254 LP – 14259.

(44) Slosky, L. M.; Caron, M. G.; Barak, L. S. Biased Allosteric Modulators: New Frontiers in GPCR Drug Discovery. *Trends Pharmacol. Sci.* **2021**, *42* (4), 283–299.

(45) Slosky, L. M.; Bai, Y.; Toth, K.; Ray, C.; Rochelle, L. K.; Badea, A.; Chandrasekhar, R.; Pogorelov, V. M.; Abraham, D. M.; Atluri, N.; Peddibhotla, S.; Hedrick, M. P.; Hershberger, P.; Maloney, P.; Yuan, H.; Li, Z.; Wetsel, W. C.; Pinkerton, A. B.; Barak, L. S.; Caron, M. G. β-Arrestin-Biased Allosteric Modulator of NTSR1 Selectively Attenuates Addictive Behaviors. *Cell* **2020**, *181* (6), 1364-1379.e14.

(46) Ullah, R.; Shah, M. A.; Tufail, S.; Ismat, F.; Imran, M.; Iqbal, M.; Mirza, O.; Rhaman, M. Activity of the Human Rhinovirus 3C Protease Studied in Various Buffers, Additives and Detergents Solutions for Recombinant Protein Production. *PLoS One* **2016**, *11* (4), e0153436–e0153436.

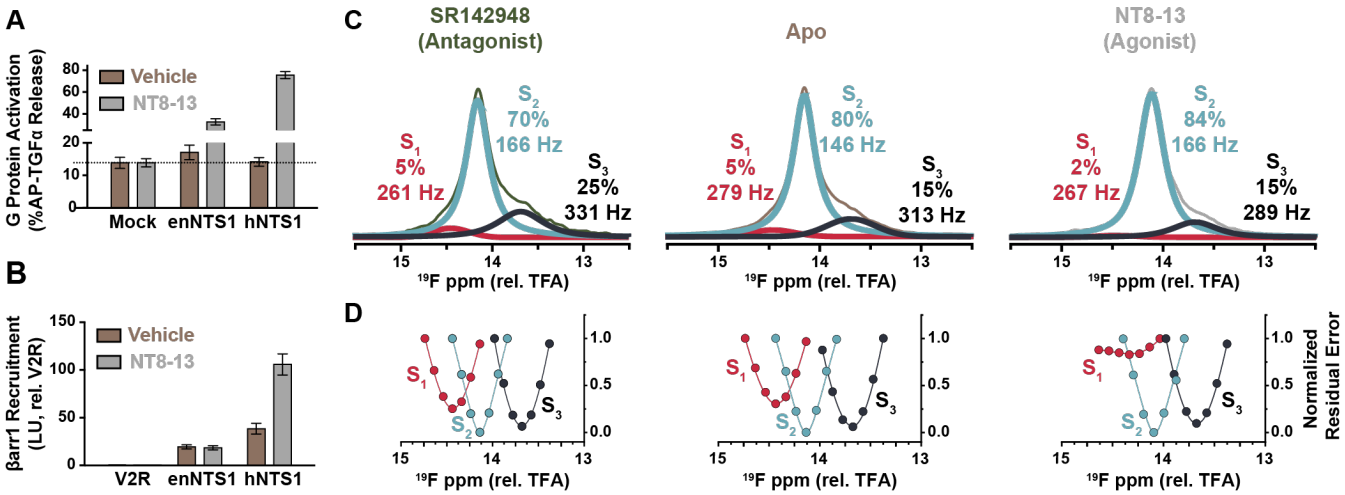

Figure 1. Orthosteric ligands modulate the enNTS1 conformational ensemble. (A) G protein activation was assessed using a TGFα shedding assay on HEK293A cells transiently-transfected with vasopressin receptor 2 (V2R; Mock), human (h)NTS1, or enNTS1.[20] Cells were stimulated with vehicle (black) or 1 μM NT8-13 (blue). Error bars represent SEM from three independent experiments. (B) βArr1 recruitment to V2R (Mock), hNTS1, and enNTS1 was measured using a NanoBiT-based assay.[22] Cells were stimulated with vehicle (black) or 1 μM NT8-13 (blue). Luminescence counts recorded from 5-10 min following stimulation were averaged and normalized to the initial counts. Error bars represent SEM from four independent experiments. (C) Deconvoluted ^{19}F-NMR spectra of enNTS1[Q301C^{BTFMA}] in various liganded states. All ligands added in 10x Meq to receptor. The relative population and LWHH are indicated for each substate. (D) The chemical shift value of each deconvoluted resonance was confirmed by monitoring the residual error while constraining peak height and LWHH. The chemical shift was constrained to a new value and the procedure repeated. The lowest residual error value for each substate represents the chemical shift used in deconvolution.

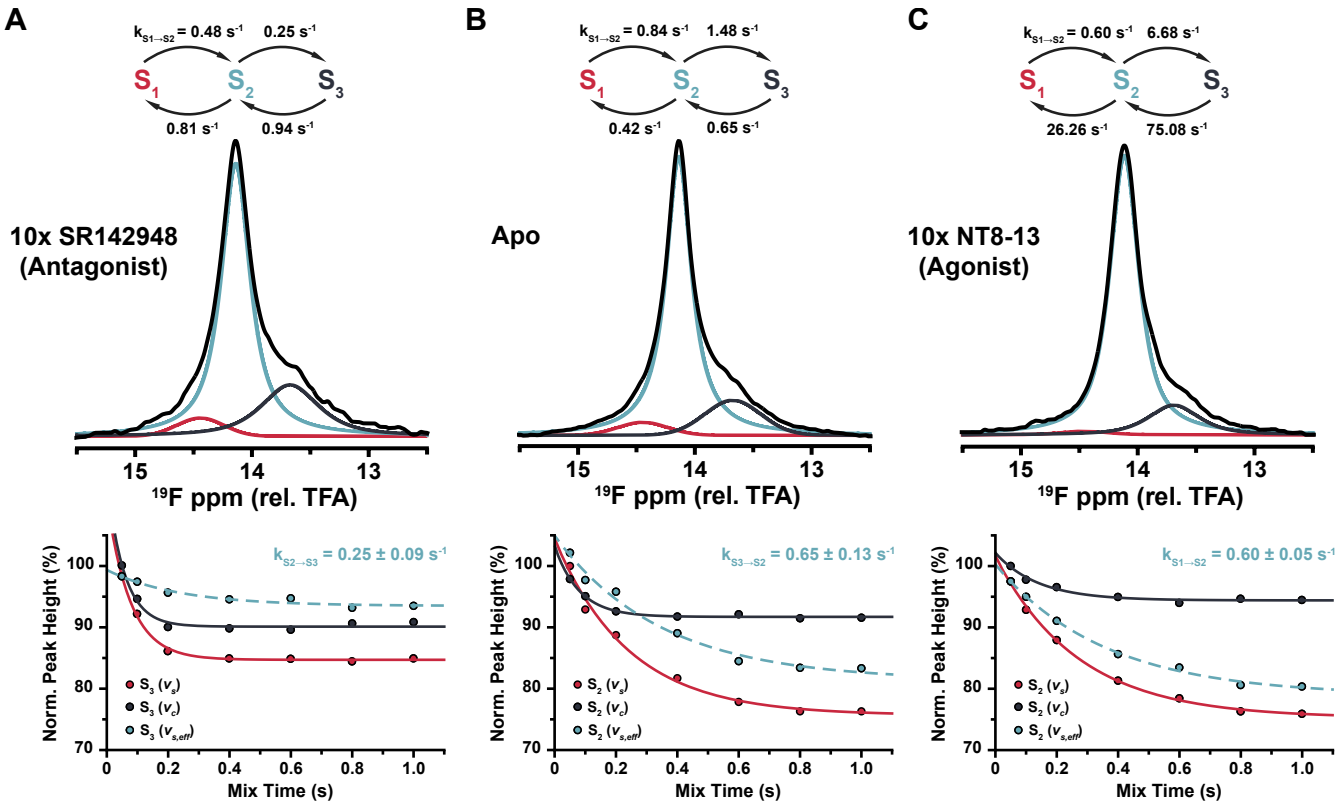

Figure 2. enNTS1 conformational substate lifetimes influenced by ligands. Deconvoluted ^{19}F-NMR spectra of enNTS1 in the absence or presence of 10 Meq ligand. Representative STD decay curves are reproduced under their respective condition in which the substate peak height following on-resonance saturation (v_s; red); the substate peak height following equidistant off-resonance saturation (v_c; slate); and the effective saturation curve ($v_{s,eff}$; dashed teal) are plotted. The effective saturation curve is calculated as the difference of on- and off-resonance saturation. This is fitted to the Bloch-McConnell equations to calculated exchange rates (k) and life-times ($\tau = 1/k$).

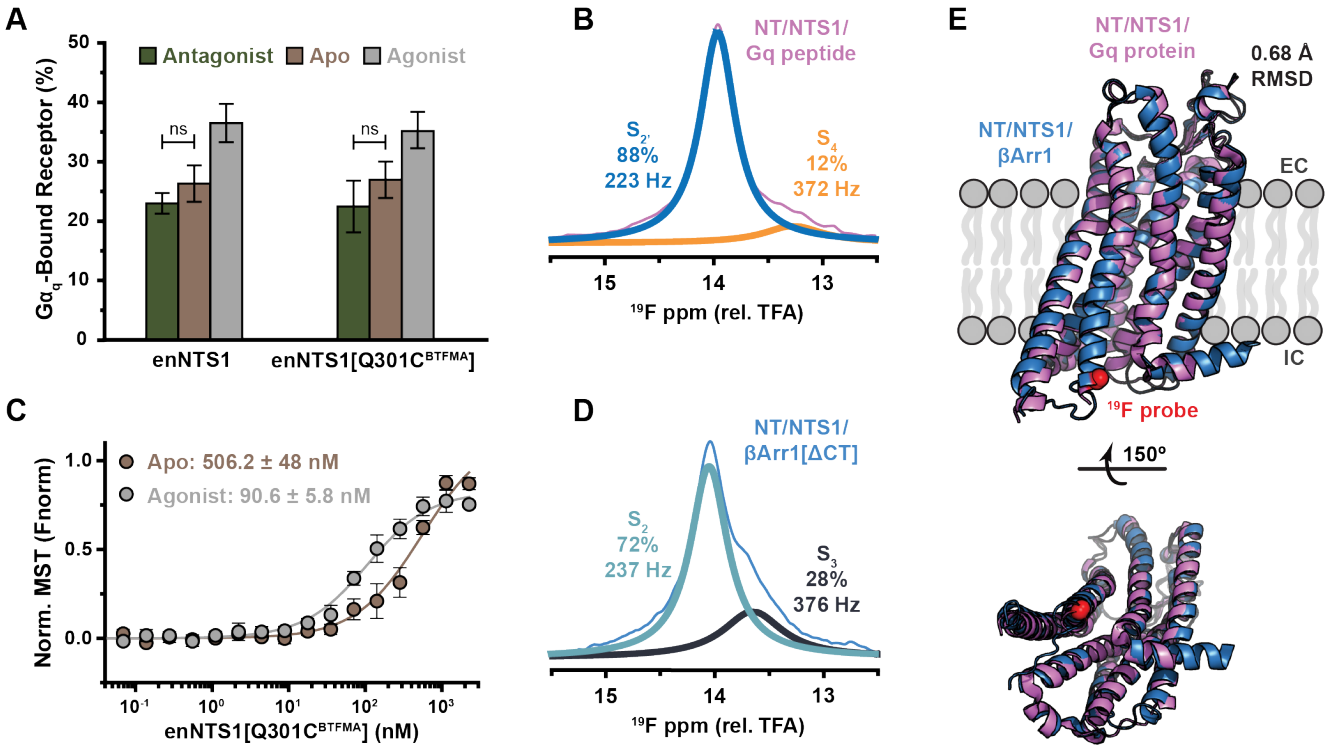

Figure 3. $G\alpha_q$ peptide and βArr1 stabilize distinct enNTS1 substates. (A) Binding of the $G\alpha_q$ peptide to enNTS1 and enNTS1[Q301C^{BTFMA}] was measured using a Dynabead sequestration assay.[35] Ligands were incubated at 10 Meq and $G\alpha_q$-bound receptor calculated as the ratio of input:bound receptor. Bars represent the average bound percentage from both experimental and instrumental triplicates; error bars represent the standard deviation. Statistical significance between conditions was calculated at P = 0.05 using a one-way ANOVA test; "ns" denotes no significance between two conditions as determined via calculated F-ratio at P = 0.05. (B) Deconvoluted ^{19}F-NMR spectra of enNTS1[Q301C^{BTFMA}] in the presence of 10 Meq NT8-13 and 5 Meq $G\alpha_q$ peptide. Two Lorentzian lineshapes ($S_{2'}$ and S_4) provided the best fit to the experimental data. (C) The affinity (K_d) of NT8-13-bound enNTS1[Q301C^{BTFMA}] for βArr1[ΔCT] was measured using microscale thermophoresis (MST). Fluorescent NTA-labeled βArr1[ΔCT] (25 nM), NT8-13 (22.5 μM), and 10x Meq PIP_2 were incubated with increasing concentrations of enNTS1[Q301C^{BTFMA}]. Data points represent the average normalized MST signal from data collected in both experimental and instrumental triplicates; error bars represent the standard deviation. Equilibrium dissociation constants were calculated from a global fit of experimental data using the quadratic binding model. (D) Deconvoluted ^{19}F-NMR spectra of enNTS1[Q301C^{BTFMA}] in the presence of 10 Meq NT8-13, 10 Meq PIP_2, and 5 Meq βArr1[ΔCT]. Two Lorentzian lineshapes (S_2 and S_3) provided the best fit to the experimental data. (E) Overlay of NTS1 receptor from NTS1:heterotrimeric Gq protein (PDB 6OS9; magenta) and NTS1:βArr1 (PDB 6UP7; blue) complex structures. Transducer and agonist were removed for clarity. The distance between Q301 in the two structures is 0.8 Å and the all-atom RMSD = 0.68 Å as calculated using PYMOL.

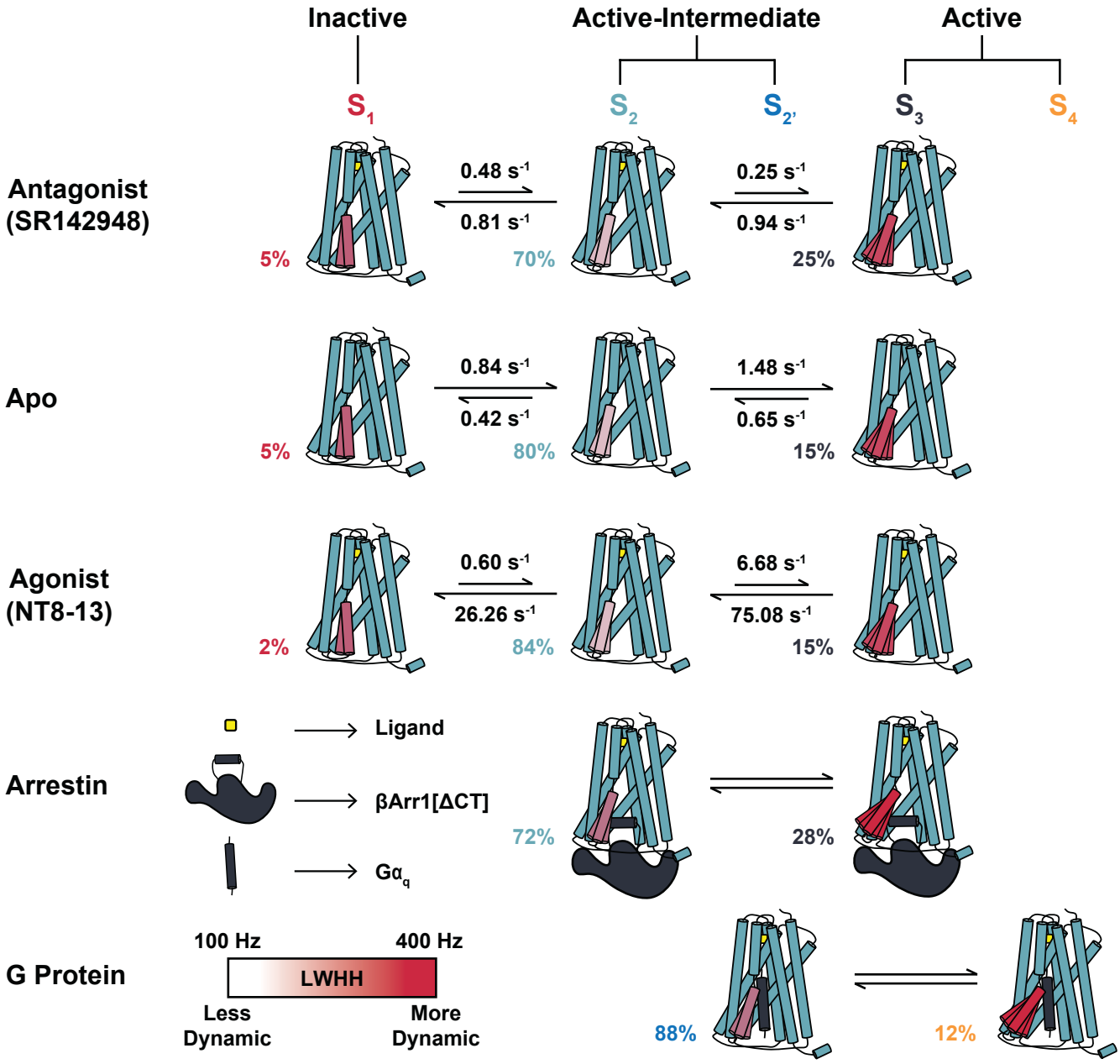

Figure 4. Model of enNTS1 substates identified by ^{19}F-NMR and the effect of orthosteric ligand or transducer on the conformational lifetime, population, dynamics, and exchange equilibrium.